

CFD Analysis of Tip Clearance Effects on the Performance of Transonic Axial Compressor

M. U. Sohail^{a,*}, H. R. Hamdani^{b,**}, and Kh. Pervez^{b,***}

^aDept. Aerospace & Aeronautics, Institute of Space Technology, Islamabad, 44000 Pakistan

^bAerospace & Aeronautics, Institute of Space Technology, Islamabad, 46000 Pakistan

*e-mail: engr.mu.sohail@gmail.com

**e-mail: hraza@hotmail.com

***e-mail: khalidparvez2009@hotmail.com

Received April 24, 2019; revised July 22, 2019; accepted August 6, 2019

Abstract—Ongoing development concerning to increase engine thrust to weight ratio in a gas turbine engine which gives rises to extremely loaded compressor stages. Highly loaded compressors stability is associated with low energy tip leakage flow (TLF) which leads to the flow blockage and thermodynamic losses. This causes greater adverse effects in transonic axial flow compressors owing to the interaction of shock wave and tip leakage flow. The current paper aims for a detail investigation of tip clearances flow field region and their profound effects on aerodynamic performance, stability range and stability margin of low aspect modern transonic axial flow compressor through mathematical modeling and numerical simulation using ANSYS CFX software. Detail rotor flow field was numerically and computationally investigated at zero tip clearance, above and below of design tip clearance to conclude the performance of compressor at suitable tip clearance. A mathematical model has been established to predict the behavior of compressor rotor at choking, peak efficiency and near stall point mass flow rate conditions at different tip clearances. Mathematical model is developed to predict the behavior of compressor at different tip clearances. Furthermore, mathematical-based model results are validated with the computational results. The eminence of both model prediction and the numerical solution was assessed, and conclusions were drawn.

Keywords: transonic compressor, tip clearances, tip leakage flow, stall margin, stability range, CFD analysis

DOI: 10.1134/S0015462820010127

NOMENCLATURE

| | |
|----------|---------------------|
| D | Design |
| m^0 | Mass flow rate |
| R | Gas constant |
| TC | Tip clearance |
| TR | Temperature ratio |
| PR | Pressure ratio |
| γ | Specific heat ratio |
| Ω | RPM |
| π | Pressure ratio |
| η | Efficiency |

Subscript “c,” “p,” “s,” shows choking, peak efficiency and near stall conditions, respectively

The nature of the flow at the blades in an axial compressor is dependent on various parameters like inlet conditions and geometry. One of the dominant geometric parameters is the tip clearance (TC) between the rotor blades and the casing wall. The flow is initiated by the clearance between the blade tip and the casing wall that encircle the whole rotor blade. The tip leakage flow is produced due to the static pressure difference from both suction and pressure sides of the blade, and the relative motion between the blades and the adjacent walls. Due to the interaction of free stream velocity that ignores the presence of gap between the blade and the wall casing and the tip leakage velocity that is perpendicular to streamwise direction incites the flow irregularly. As a result, this leakage may induce the vortices on the suction side of the blade that disturb the incoming flow. Gegg et al. [1] proposed that the two crucial factors that control the tip leakage flows are the magnitude of the TC gap and the blade loading, i.e., the static pressure difference between the suction and pressure side of the blade). Peacock [2] proposed that an increase in the TC gap between the blade and the casing wall poses a detrimental effect on the compressor efficiency, pressure rise, flow losses and compressor performance as there may be no work done physically on flow by the blades. Hewkin-Smith et al. [3] experimentally proved that compressor performance is deteriorated by increasing the tip clearance. Due to small clearance Reynolds number and small length available for transition to turbulent flow, the laminar flow may occur in the tip clearance region. Whereas, large boundary layer flow variation may occur by relatively small tip leakage flow. Schulz et al. [4] proposed that flow separation at TC region is not due to the clearance effect however, it depends upon the magnitude of blending effects of secondary flows and leakage flows. Xiao et al. [5] explained the previous researches on secondary flows, that it enforces the Boundary layer to move towards the suction surface. Whereas, leakage flow restrains this flow to accumulate at the corner formed by the wall and blade suction surface. Among the pressure surface due to TC the deviation of flow along the pressure surface of the blade is greater than without TC. Whereas, the flow on the suction surface of the blade is towards the tip region. Flow losses in turbomachinery occur due to the interaction of secondary flows and main flow. Walsh [6] classified the flow losses in turbomachinery as following

- *Profile losses*: Associated with the viscosity of the fluid here, entropy increases due to the presence of the wall boundary layer and mixing layer that contribute mechanical energy dissipation into heat, whereas, total pressure decreases that reduces the work output and efficiency of the compressor.
- *Shock losses*: An increase of static pressure across the shock waves further thickens the boundary layer that generates adverse flow pressure, therefore, causes early flow separation.
- *Secondary flow and end wall losses*: Arise due to the interaction of the boundary layer with all kinds of vortices such as passage vortex, scrapping vortex and corner separation. Scrapping vortex develops due to the relative motion between the blade and the casing wall. Similarly, corner separation becomes dominant when the leakage flow leaves the suction surface end due to the presence of an adverse pressure gradient.
- *Clearance losses*: Arises due to the increase of TC between the rotating blade and the wall casing reduces the work output and efficiency of the compressor.

Adamczyk et al. [7] studied the 3D Navier–Stokes numerical simulation of the axial compressor rotor to investigate the flow instability at the tip region of the high-speed rotor. He concluded that at zero clearance computation showed a higher flow range than non-zero TC. Whereas at non-zero TC a low energy fluid was developed due to the interaction of in-passage shock and clearance vortex. Neise and Wolfgang [8] investigated both numerically and experimentally the cause of unsteadiness of flow behavior and revealed that flow vortex developed near the leading edge of the blade is due to the interaction of incoming flow, TC flow, and secondary flow. Hah et al. [9] analyzed that a large percentage of aerodynamic losses occur near the rotor tip section in the transonic compressor. Their research proposed that, when rotor operates at normal, maximum polytropic efficiency and even near stall point condition the TC vortex does not break down. The result shows that the flow field becomes unsteady due to shock oscillation even though the TC vortex does not break down. Yamada et al. [10] investigated the separated flow fields and vortices at different TCs cases between the rotor blade and wall casing through RANS steady and unsteady simulation. He concluded that due to the formation of shock waves and vortex interaction near the stall condition breakdown of tip-leakage vortex occurs.

Wu et al. [11] investigated the unsteady behavior of Tip leakage flow and concluded that unsteadiness is caused by the cyclical motion of tip secondary vortex. Gbadebo et al. in 2007 [12] and Danish et al. in 2016 [13] explained the relation of tip clearance flow with 3 D flow separations of a compressor cascade corner region. According to his research by introducing small clearance between the stationary hub and the blade, separation of flow on the blade suction side can be removed. Tan et al. [14] experimental investigated on tip leakage vortex and turbulence of an axial compressor by refractive index methodology. He utilized the NaI solution for unhindered PIV measurement. He deduced that flow separation is caused

due to the interaction of passage flow and leakage flow. At near the stall condition flow leakage restricted towards the leading edge and moves faster towards the pressure side of the next blade. Furthermore, within the blade passage, TLF does not breakdown into a single vortex whereas it tends to breakdown after the path of the rotor passage. Heinlein et al. [15] employed a statistical analysis method to predict the stall precursor and analyzed flow physics on stall inception. Their research illustrated statistical Grubb's trends to predict the early rotating stall in the transonic compressor stage 35. Whereas, Grubb's pattern moved slower and faster than the rotor speed was exposed due to the consequence of flow blockage in blade passage, amid motions in the breakdown of the tip clearance vortex and higher blade loading and axial pressure respectively. Zhuang and Liu [16] introduced CLES (Reynolds-stress constrained large eddy simulation) method for tip leakage flow behavior investigation at near stall condition. Their research shows three dissimilar flow fluctuations regions formed on the suction side, blade passage and ahead of the leading edge of the rotor blade tip. In [17], time dependent simulation was conducted in order to capture unsteady flow phenomenon of Rotor 67. Their research explained different types of compressor flutters, mainly stall flutter that causes compressor blade failure. Furthermore, their research focused on the tip clearance availability discrepancies.

1. PHYSICAL PROBLEM

NASA transonic compressor Rotor 67 is a first stage rotor designed for two stage fans. Due to its high mass flow rate and designed pressure ratio, it is widely researched in the aerospace industry. Hah et al. [9] studied the flow field near the casing of a forward swept transonic compressor Rotor 37. He investigated the flow structure with nominal and with zero tip clearance flow and its interaction with the passage shock. Strazisar et al. experimentally conducted research on "Laser Anemometer Measurements in a Transonic Axial Flow Fan Rotor" at NASA Lewis Research Center [18] proposed rotor 67 geometry and designed tip clearance of 1.016 mm. Abate [19] carried out Bezier curves and GA for an optimization technique of Rotor 67 at 1.016 mm tip clearance. Drayton [20] experimentally investigated the advantages of splitter blade geometry, and placement for compressor rotor 67 with 0.91 mm tip clearance in order to increase the mass flow range without the loss of pressure ratio. Mehdi [21] investigated swirl distortion, and its adverse effects on engine performance of turbofan compressor Rotor 67. He used 0.6 mm tip clearance with bulk swirl flow and flow incidence on the blade. This results in reduction of the mass-flow rate, therefore, deteriorates the compressor performance.

So far, there is no published work that relates the comprehensive analysis on the tip clearances and its effect of compressor Rotor 67 stability range and stall margin. The research aims to study the flow physics at eight different TC region of NASA Rotor 67 computationally and generate set of polynomial equations to reduce the computational time and to predict the behavior of rotor at different TC regions. Furthermore, optimal TC is suggested based on current research for NASA Rotor 67 to maximize its pressure ratio while satisfying all geometrical and performance constraints.

In the first part of the research detailed flow physics has been discussed at eight different TCs, i.e., at 0, 0.6, 0.8, 0.9, 1.016, 1.2, 1.6, 2.0, and 2.5 mm. In the second part of the research 3rd order polynomial equation has been generated by compressor characteristic map to predict the compressor characteristic numerically at choking, peak efficiency and near stall point regions. Both numerical and computational results are later validated with NASA experimental data. In the third part of the research stability margin and stability range of the compressor rotor has also been investigated at different TC.

2. COMPUTATIONAL SETUP

Transonic compressor NASA rotor 67 is composed of 22 blades and at leading and trailing edges having 25.7 and 24.25 cm tip radii, respectively. The revolution about the negative Z axis has been generated. Three dimensional steady compressible Navier–Stoke equation has been solved using the $K-\epsilon$ turbulence model. At the boundaries of the rotor computational domain, standard boundary conditions are applied. Whereas, no-slip conditions are used on walls and periodic conditions are applied at the periodic surfaces. Sutherland viscosity law with three coefficients for ideal gas has been applied. In the current study, ideal air gas is chosen to describe the fluid. At the rotor inlet boundary conditions, the total pressure is 1atm, the total temperature of 288.15 K, and flow direction were specified. Whereas at the outlet of the rotor, average static pressure was specified. The computation is carried out at design RPM of 16 043. 3D mesh at coarse, medium, fine and the super fine mesh has been generated. For grid analysis computation is carried

Table 1. Mesh independent study

| Sr. no. | Mesh quality | Nodes | Designed mass flow rate |
|---------|--------------|---------------|-------------------------|
| 1 | Coarse | 37156 | 33.43 |
| 2 | Medium | 159096 | 33.64 |
| 3 | Fine | 398274 | 33.54 |
| 4 | Very Fine | 958784 | 33.14 |
| 5 | Super Fine | 1466255 | 33.14 |

out to 0.4 to 1.6 million mesh nodes. Computations are performed at tin 288.15 K and 16043 RPM. The result shows that the fine hexahedral-grid mesh with 0.96 million mesh elements has a decent compromise between computational and experimental results as shown in Table 1.

3. RESULTS AND DISCUSSION

3.1. Validation

Computation was carried out from choking condition to near stall condition by gradually rising outlet average static pressure to obtain compressor rotor characteristic graph. The near stall point was predicted at the last stable condition of the Rotor 67. Figures 1a and 1b shows a characteristic map among normalized mass flow rate vs pressure ratio and adiabatic efficiency of the compressor at designed RPM and TC 1.016 mm, respectively. Results illustrate good validation between computational and NASA experimental results Strazisar et al. [18].

Table 2 shows the maximum and peak mass flow rate difference between computational and NASA experimental results at deigned TC of 1.016 mm and RPM 16 043. Results validate a decent justification with the NASA results at designed conditions. Furthermore, the table also shows the computational difference of mass flow rate at different tip clearances from the computational designed 1.016 mm TC mass flow rate.

Figure 2 shows relative Mach number contours distribution at 70% span for both at peak efficiency and near stall operating conditions at design TC 1.016 mm of the author(s) computational results with NASA experimental results. Both computational and experimental results show that the inlet Mach number is subsonic. Whereas, experimental results show normal shock around the LE at both conditions and a high number of relative Mach number after the normal shock. Flow fields feature between both operating conditions are very similar and show agreement between the computational and experimental results.

3.2. Results at Design TC

Figures 3a and 3b show static temperature contours at the pressure and suction sides of the blade at the designed clearance of 1.016 mm. Results show a very low region of temperature contours near the hub of the blade. The temperature gradually starts increasing at mid of the span and there is a high-temperature region at the TE on the pressure side of the blade. Whereas, the temperature contour shows almost similar

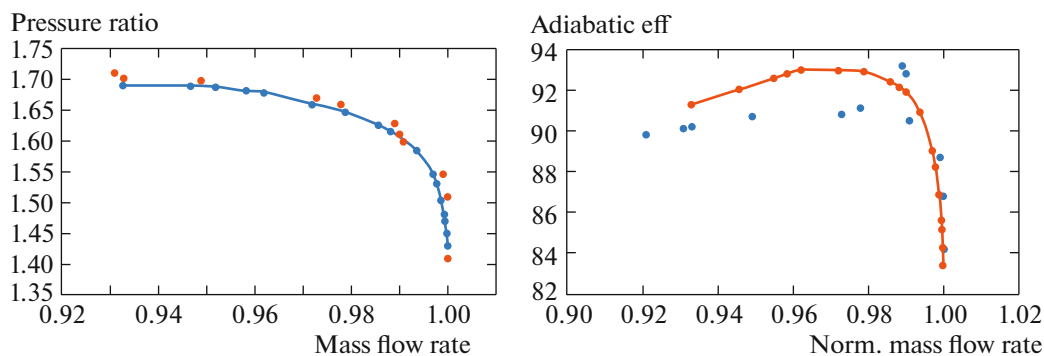


Fig. 1. Characteristic maps. —●—, Computational; ●, NASA experimental.

Table 2. Computational mass flow rate differences

| Tip clearance, mm | Mc diff., kg/s | Mp diff., kg/s |
|-------------------|----------------|----------------|
| 0.6 | 0.015 | -0.007 |
| 0.8 | 0.014 | -0.011 |
| 0.9 | 0.014 | -0.001 |
| 1.016 | 0.015 | 0.003 |
| 1.2 | 0.015 | 0.004 |
| 1.6 | 0.016 | -0.008 |
| 2 | 0.017 | -0.008 |
| 2.5 | 0.018 | -0.020 |

behavior at the suction side of the blade where there is a high-temperature region above 90% span of the blade.

Figures 3c and 3d shows Mach number contours at the pressure and suction side of the blade at designed TC 1.016 mm. Results show that the Mach number remains subsonic near the hub of the blade. Flow becomes transonic at nearly 50% span of the blade and 90% span of blade flow becomes nearly supersonic at the LE of the suction side. Whereas, flow behavior at the pressure side is almost similar to the suction side of the blade.

Figures 3e and 3f show the pressure contours at the pressure and suction side of the blade. Results show that pressure gradually rises from hub to shroud as there is a low-pressure region near the hub of the blade and the very high-pressure region above 80% span on the pressure side of the blade. At the suction side of the blade pressure behavior shows similar behavior near the hub region and there is a visible high-pressure region at the TE of the blade.

3.3. Result at TC lesser than Design

In comparison with design TC of 1.016 mm, the following computational trends have been seen at blade suction and pressure side at four tip clearances (0, 0.6, 0.8, 0.9 mm) which are lesser than the

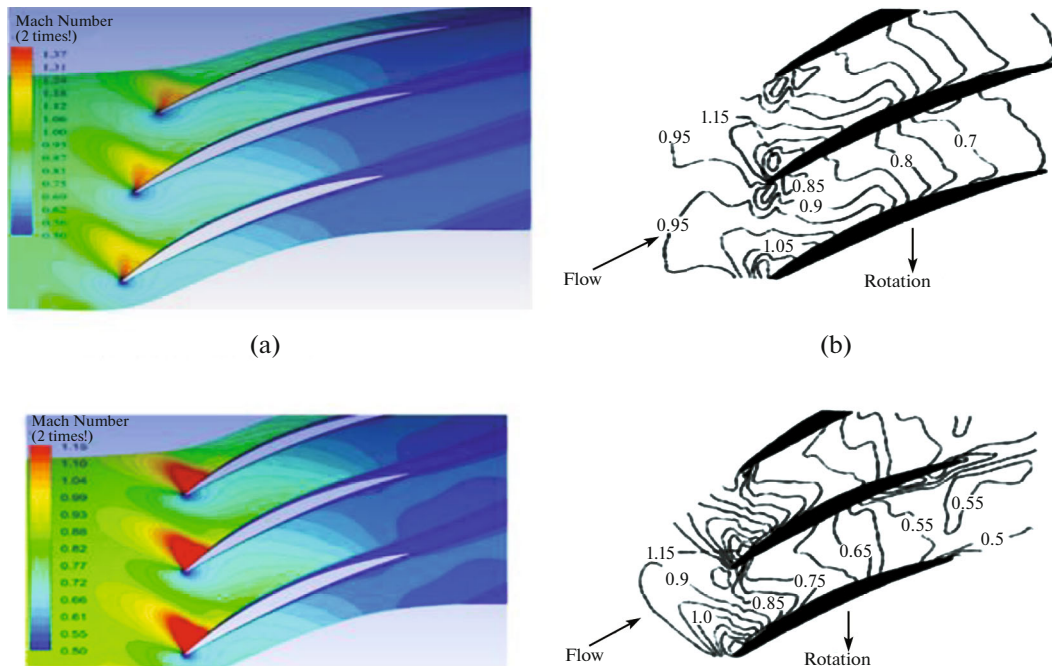


Fig. 2. Validation blade to blade Mach contours at peak efficiency (at the top) and for near stall condition (at the bottom): (a) Computational 70% span Mach contours, (b) NASA Experimental 70% span Mach contours.

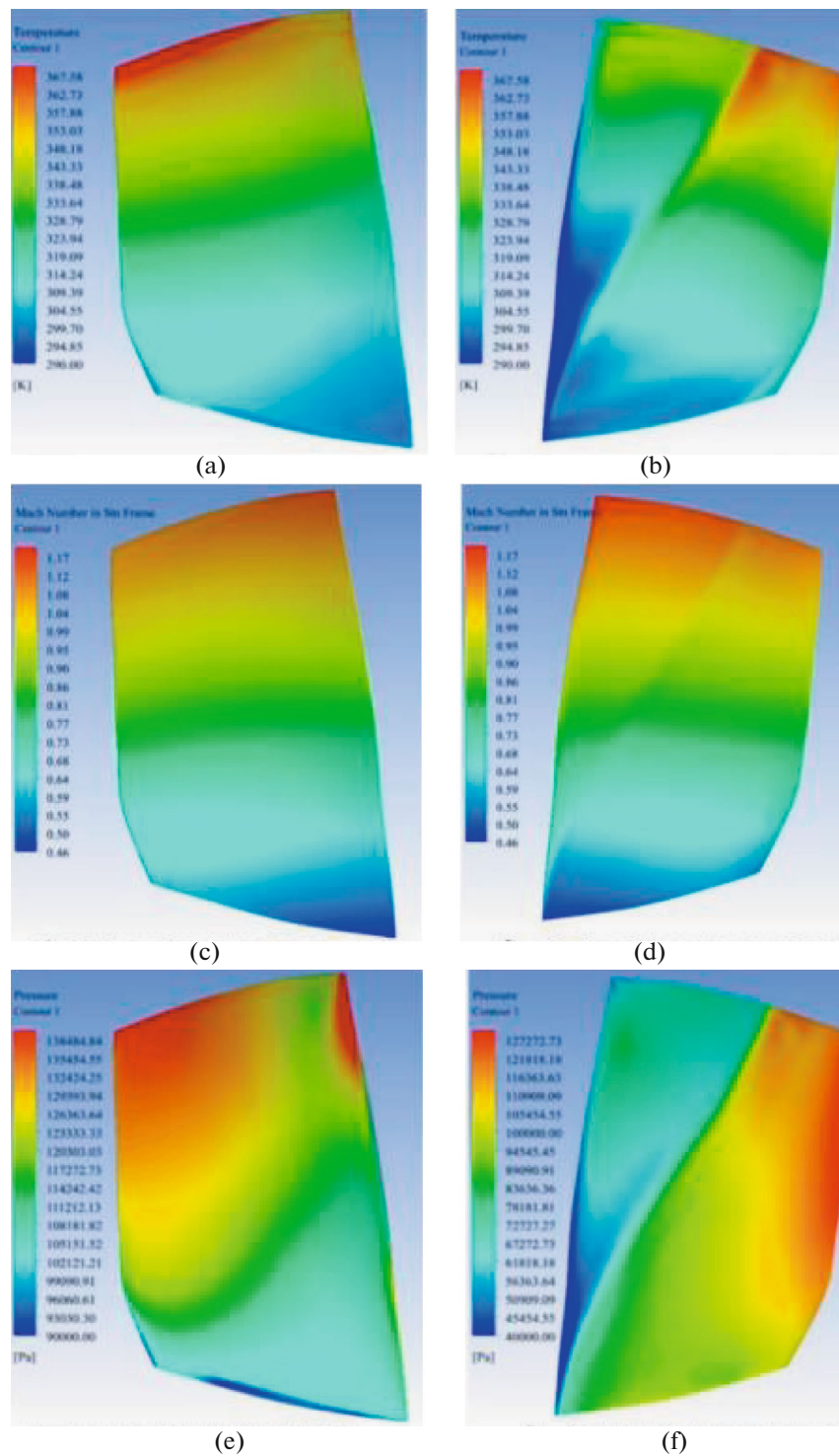


Fig. 3. Flow contours at design tip clearance: (a) temperature profile at pressure side, (b) temperature profile at suction side, (c) mach number profile at pressure side, (d) mach number profile at suction side, (e) pressure profile at pressure side, (f) pressure profile at suction side.

designed TC. Temperature contours in Figs. 4a and 4b show almost similar behavior of both suction and pressure side of the blade with design TC (Figs. 3a and 3b). Whereas, stronger oblique shock at tip core is seen at lower TC which gradually moves towards the trailing edge of the blade as clearance increases till the designed TC. Mach number contours in Figs. 4c and 4d also show similar behavior of designed TC

(Figs. 3c and 3d). Designed TC shows a greater extent of a supersonic region than lesser TC at LE of the suction side of the blade. Whereas, on blade suction side of lesser TC oblique shock is stronger at the LE of tip region. Pressure contours in Figs. 4e and 4f show similar behavior of both suction and pressure side at near the hub to mid of the span of the blade with design TC (Figs. 3e and 3f). A very high-pressure region is seen at the TE near the tip region of TC lesser than the design at both suction and pressure side of the blade. Whereas, the pressure region near the tip region starts decreasing by increasing the TC till the designed.

Figures 4g and 4h show tip leakage flow behavior of a compressor rotor at TC lesser than designed TC. Computational results show similar behavior as proposed by Hah et al. [9] for transonic compressor. Results show that due to shock oscillation flow becomes unsteady whereas, TC vortex does not break down. At zero TC no particles can flow over the blade towards the low momentum area.

3.4. Result at TC Greater than Design

Figure 5 shows temperature, Mach number, and pressure contours for TC greater than the designed tip clearance at suction and pressure side of the rotor. It is seen that for TC greater than the design TC, the generated trend is as follows:

- Temperature contours (Figs. 5a, 5b) show that the entire blade has very weak temperature regions at the suction side of the blade. Whereas, at LE of blade pressure side temperature starts diminishing as TC increases.
- Mach number contours (Figs. 5c, 5d) show slightly supersonic flow near the tip, as it increases by increasing the tip clearance than the designed. Furthermore, at suction side oblique shock moves towards the TE of the blade therefore, it deteriorates the compressor performance at a greater extent.
- Pressure contours (Figs. 5e and 5f) show that high-pressure region at the TE near the tip region decreases to at greater extent by increasing the tip clearance. A very weak pressure region is dominant throughout the blade. This shows massive deteriorated compressor performance at higher tip clearances than the designed.
- Figures 5g, 5h shows tip leakage flow behavior of a compressor rotor at TC greater than designed TC. Results show that by increasing the TC secondary flow becomes dominant therefore, the interaction of strong secondary flows with the passage flows results tip leakage flows

For better visualization of results, all scales considered in each figure were held constant. Mach number contours at both suction and pressure side are kept from 0.46 to 1.17. For temperature at both suction and pressure sides, contours are kept at 290 to 368 K. Whereas, pressure contours at pressure side for all results were kept at 90 000 to 140 000 Pa, and for suction sides 40 000 to 128 000 Pa.

3.5. Stability Range (SR) and Stall Margin (SM)

Figures 6a and 6b show the stability range and stall margin of compressor at different tip clearances region. Stall margin and stability range are calculated by following equations, which is defined by different researchers [22, 23]

$$SM = 1 - \left\{ \left[\frac{PR_{\text{design}}}{PR_{\text{stall}}} \right] \times \left[\frac{m_{\text{stall}}^0}{m_{\text{design}}^0} \right] \right\}, \quad (3.1)$$

$$SR = \frac{m^{\text{ochoking}} - m^{\text{osurge}}}{m^{\text{ochoking}}}. \quad (3.2)$$

Here, the design, stall, choking, and surge indices refer to calculated values of flow stall (surge), flow blocking, and peak values, respectively.

The results show that the stall range of the compressor increases from 0.6 mm TC to 1.016 mm TC. This shows 1.016 mm has maximum stability range (Fig. 6a). Whereas, by further increasing the TC, stability range of the compressor start decreasing. Figure 6b shows almost same stall margin at minimum TC. Whereas, stall margin is maximum at designed 1.016 mm TC of the compressor. Furthermore, SM deteriorated by increasing TC's. This shows that rotor with 1.016 mm tip clearance has better overall reliability and performance.

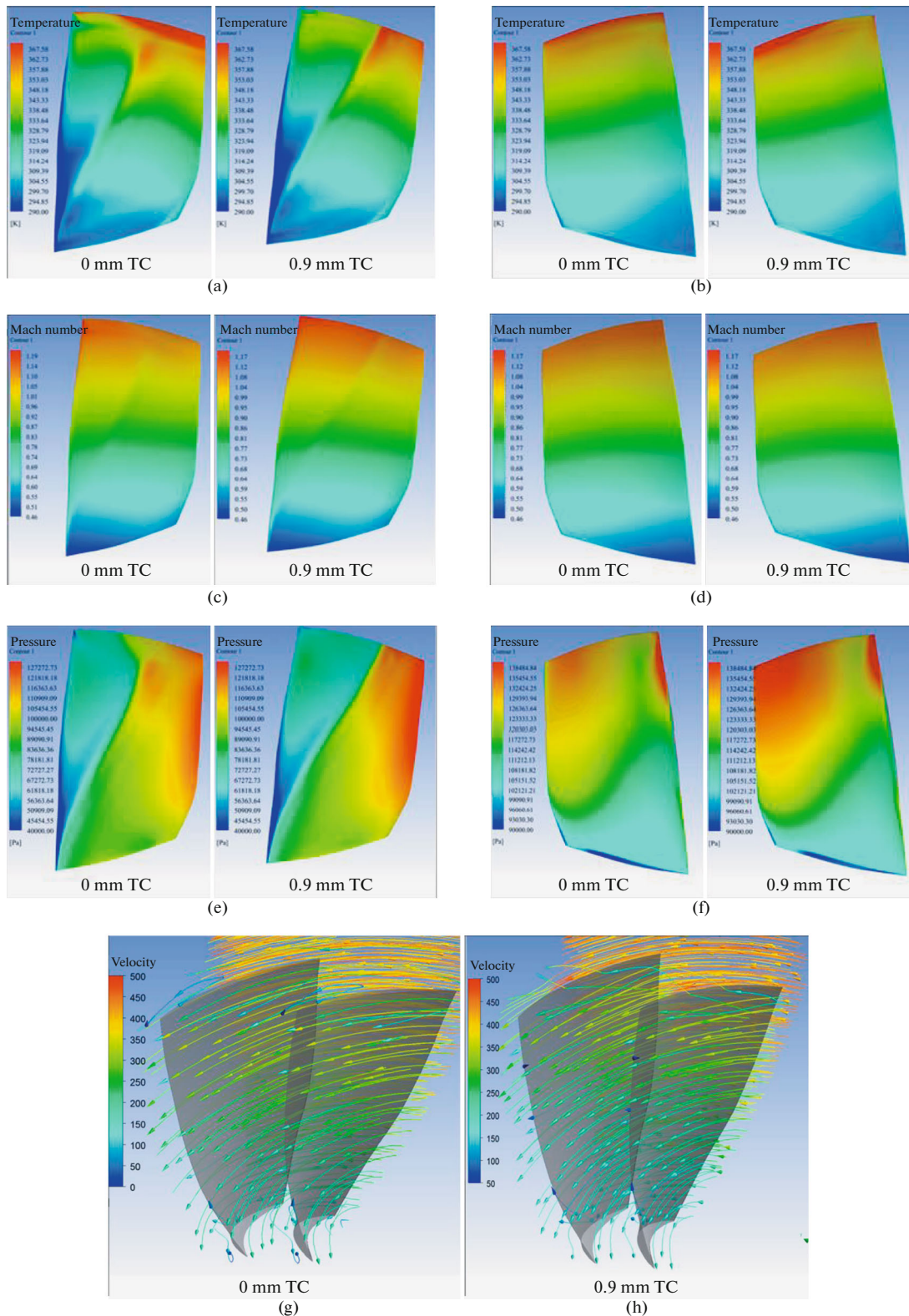


Fig. 4. Flow Contours at TC lesser than design: (a) temperature contours at less than designed TC at suction side, (b) temperature contours at less than designed TC at pressure side, (c) Mach contours at less than designed TC at suction side, (d) Mach contours at less than designed TC at pressure side, (e) pressure contours at less than designed TC at suction side, (f) pressure contours at less than designed TC at pressure side, (e, f) tip leakage flow at less than designed TC.

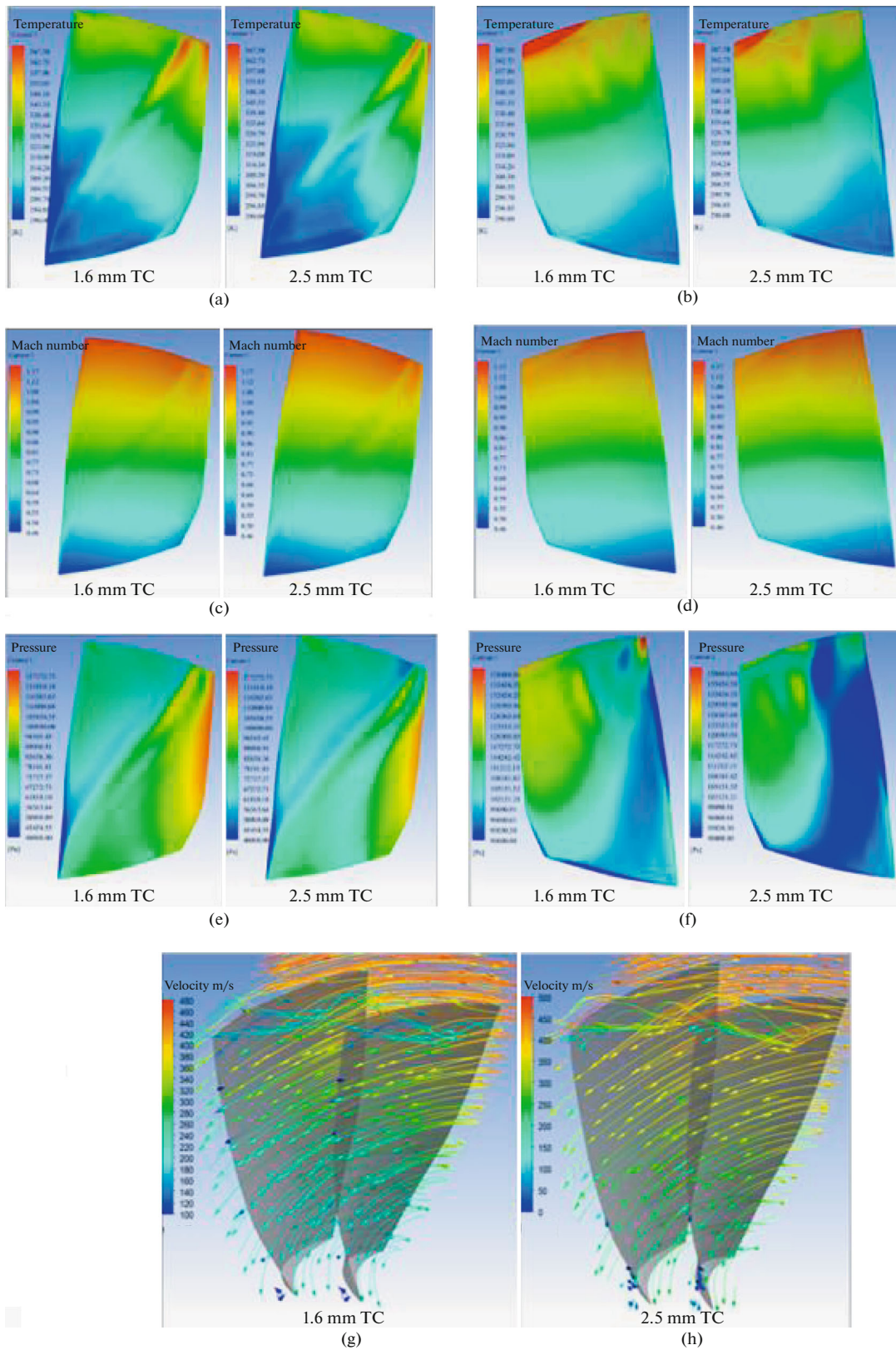


Fig. 5. Flow contours at TC greater than design TC: (a) temperature contours at more than designed TC at suction side, (b) temperature contours at more than designed TC at pressure side, (c) Mach contours at more than designed TC at suction side, (d) Mach contours at more than designed TC at pressure side, (e) pressure contours at more than designed TC at suction side, (f) pressure contours at more than designed TC at pressure side, (e, f) tip leakage flow at more than designed TC.

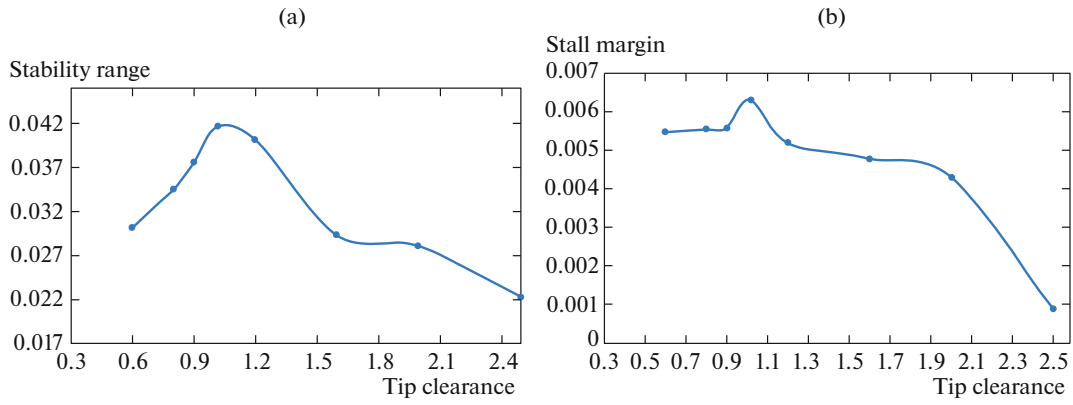


Fig. 6. TC Comparison (a) stability range (b) stall margin.

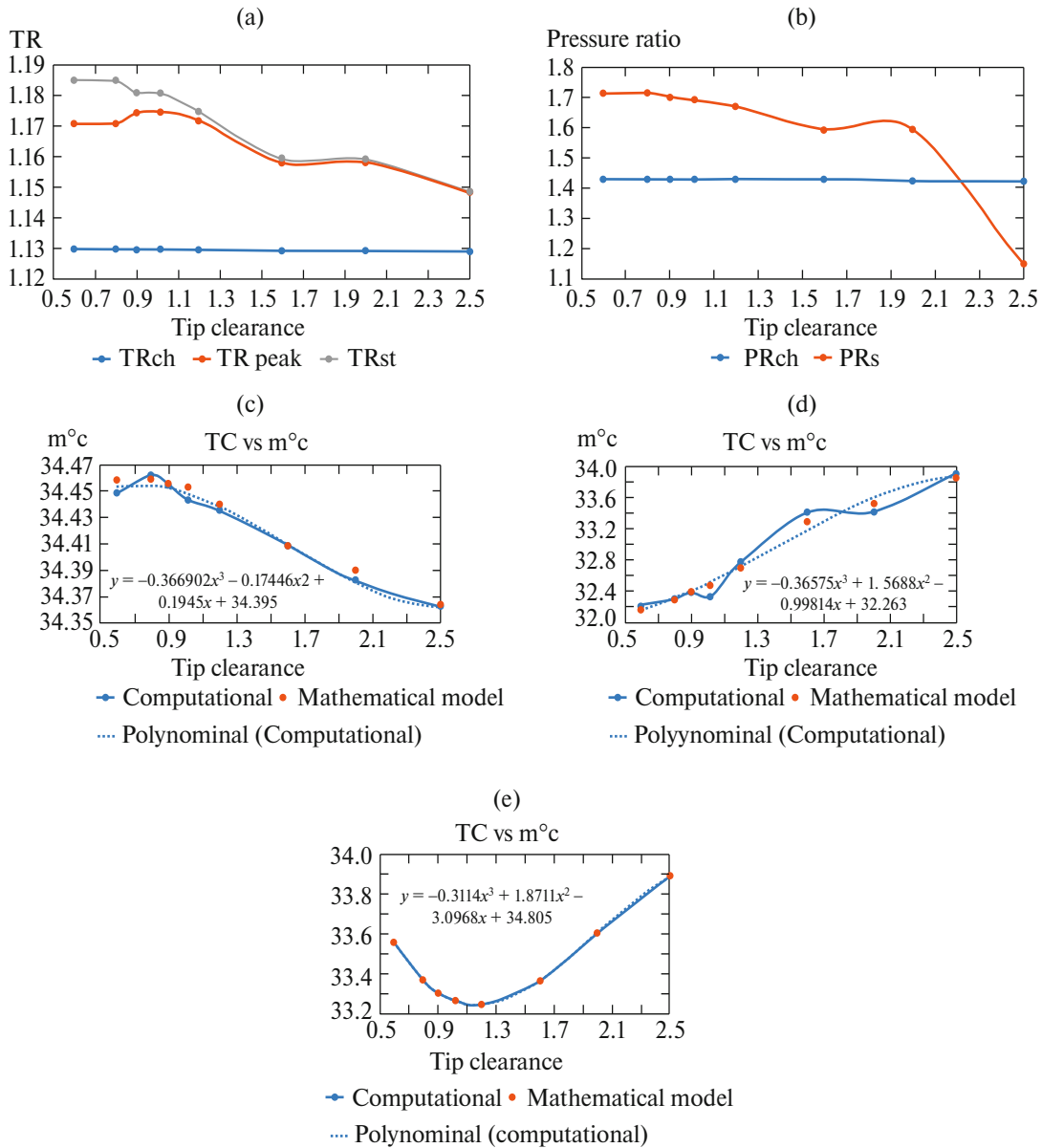


Fig. 7. Rotor performances and polynomial equation verification: (a) TC vs temperature ratio, (b) TC vs pressure ratio, (c) validation of TC vs choking mass flow rate, (d) validation of TC vs near small mass flow rate, (e) validation of TC vs peak eff mass flow rate.

3.6. Rotor Performance for Different Tip Clearances

Figures 7a and 7b illustrate the graphical representation between TC effects on temperature ratio and pressure ratio respectively. Following computational trends have been concluded:

- Temperature ratio TR_{ch} is independent of TC at choking conditions as it remains nearly constant for all tip clearances.
- Temperature ratio (TR_{peak}) is slightly higher at peak efficiency of 1.016 mm TC and gradually decreases by increasing TC.
- At near stall point, temperature ratio TR_{st} has a negligible effect at lower TC but it significantly deteriorated at higher tip clearances.
- At the choking condition, the pressure ratio PR_{ch} at 1.016 mm TC is slightly higher and it remains nearly same for all TC. At near stall point, pressure ratio PR_{st} is deteriorated by increasing the tip clearance.

Figures 7c, 7d, and 7e shows the 3rd order polynomial mathematical model verification with recent computational results as shown in Fig. 1, that predict the behavior of compressor mass flow rate at different tip clearances at choking, near stall point, and peak efficiency conditions. Whereas, the polynomial relation is used for predicting the flow behavior at above all conditions from 0.1 mm TC to 2.5 mm TC at 0.1 mm difference.

SUMMARY

One stage transonic axial compressor. with steady three-dimensional analysis is investigated for data collection as part of a larger project namely “System Identification Development for Analysis of Transonic Axial Compressor Rotor 67.” This study is concerned about the transonic compressor when subjected to have different TC region to investigate flow behavior and TLF. Following are presented:

- The TC effects compressor pressure ratio and efficiency. Therefore, investigation of acceptable tip clearance is essential during compressor design. The results and analysis explained in this work is used for that purpose.
- The increase in TC than the design TC poses a detrimental effect on the compressor efficiency, pressure rise, and performance. Results show that choking mass flow rate of the rotor decreases by increasing the TC.
- The stall margin and stability range of the transonic compressor increases from minimum tip clearance to 1.016 mm TC. Whereas, by further increasing the TC, both stability range and stall margin decreases. Therefore, it deteriorates the compressor performance.
- The stability range and stall margin of compressor at 1.016 mm tip clearance is maximum.
- Temperature ratio is independent to tip clearance at choking conditions as it remains nearly constant for all tip clearances.
- Temperature ratio is found slightly higher at peak efficiency of 1.016 mm tip clearance and gradually decreases by increasing tip clearance.
- Mach number decreases by increasing the tip clearance which result to rise of static pressure at blade suction surface.
- At zero tip clearance no particles can flow over the blade towards the low momentum area as there is no TLF interaction with the passage flow.

REFERENCES

1. S.G. Gegg, N.J. Heidegger, and R. A. Mikkelson, Computational modeling and thermal paint verification of film-cooling designs for an unshrouded high-pressure turbine blade, in *ASME, Heat Transfer; Electric Power; Industrial and Cogeneration*, Indiana, USA, 1999.
2. Peacock, A review of turbomachinery tip gap effects: Part 2: Rotating machinery, *International Journal of Heat & Fluid Flow*, 1986, vol. 4, pp. 3–16.
3. M. Hewkin-Smith, G. Pullan, S.D. Grimshaw, E.M. Greitzer, and Z.S. Spakovszky, The role of tip leakage flow in spike type rotating stall inception, in: *Turbomachinery Technical Conference and Exposition*, Charlotte, North Carolina, USA, June 26–30, 2017.
4. Schulz, H.E. Gallus, and B. Lakshminarayana, Three dimensional separated flow field in the endwall region of an annular compressor cascade in the presence of rotor–stator interaction, *Journal of Turbomachinery*, 1989, vol. 1.

5. X. Xiao, A.A. McCarter, and B. Lakshminarayana, Tip clearance effects in a turbine rotor: Part I. Pressure field and loss, *J. Turbomachinery*, 2000, vol. 123, no. 2, pp. 296–304.
6. P.P. Walsh, *Gas Turbine Performance*, Second Edition, Blackwell Science, 2004.
7. J. Adamczyk, M.L. Celestina, and E.M. Greitzer, The role of tip clearance in high speed fan stall, *J. Turbomachinery*, 1993, vol. 115, no. 1, pp. 28–38.
8. J.M. Neise, Ch. Hah, Wolfgang, An experimental and numerical investigation into the mechanisms of rotating instability, in: *ASME Turbo Expo, J. Turbomachinery*, New Orleans, Louisiana, USA, June 4–7, 2001.
9. C. Hah, D.C. Rabe, and A.R. Wadia, Role of tip leakage vortices and passage shock in stall inception in a swept transonic compressor rotors, in: *ASME Turbo Expo 2004: Power for Land, Sea, and Air*, Vienna, Austria, June 14–17, 2004.
10. K. Yamada, M. Furukawa, T. Nakano, M. Inoue, and K. Funazaki, Unsteady three-dimensional flow phenomena due to breakdown of tip leakage vortex in a transonic axial compressor rotor, in *ASME Turbo Expo 2004: Power for Land, Sea, and Air*, Vienna, Austria, June 14–17, 2004.
11. Y. Wu, Q. Li, J. Tian, W. Chu, Investigation of pre-stall behavior in an axial compressor rotor. Part I: Unsteadiness of tip clearance flow, *J. Turbomachinery*, 2012, vol. 134, no. 5.
12. S.A. Gbadebo, N.A. Cumpsty, and T.P. Hynes, Interaction of tip clearance flow and three dimensional separations in axial compressors, *J. Turbomachinery*, 2007, vol. 129, pp. 679–685.
13. S.N. Danish, S. Qureshi, M.M. Imran, S. Din Khan, A. El-Leathy, H. Al-Ansary, and M. Wei, Effect of tip clearance and rotor-stator axial gap on the efficiency of multistage compressor, *Applied Thermal Engineering*, 2016, pp. 988–995.
14. D. Tan, Yu. Li, H. Chen, I. Wilkes, and J. Katz, The three dimensional flow structure and turbulence in the tip region of an axial flow compressor, in: *ASME Turbo Expo, Turbine Technical Conference and Exposition*, Montreal, Quebec, Canada, June 15–19, 2015.
15. G.S. Heinlein, J.P. Chen, C.M. Chen, S. Dutta, and H.W. Shen, Statistical anomaly based study of rotating stall in a transonic axial compressor stage, in: *ASME Turbomachinery Technical Conference and Exposition, Volume 2D*, Charlotte, North Carolina, USA, June 26–30, 2017.
16. Yu. Zh. Liu and Hui, Prediction of unsteady tip leakage flow of a transonic compressor rotor by Reynolds-stress-constrained large eddy simulation, in: *ASME: Turbomachinery Technical Conference and Exposition*, Vol. 2A, Oslo, Norway, June 11–15, 2018.
17. R.W.A. Turan and A.A. Turan, Simple approach to computational aeroelasticity of NASA Rotor 67, in: *29th Congress of the International Council of the Aeronautical Sciences (ICAS)*, St. Petersburg, 2014.
18. A.J. Strazisar, J.R. Wood, M.D. Hathaway, and K.L. Suder, *Laser Anemometer Measurements in a Transonic Axial-Flow Fan Rotor*, NASA Scientific and Technical Division, Lewis Research Center, Cleveland, Ohio, 1989.
19. G. Abate, *Aerodynamic Optimization of a Transonic Axial Compressor Rotor*, Universita' Degli Studi Di Padova, Italy, 2012.
20. S. Drayton, *Design, Test, and Evaluation of a Transonic Axial Compressor Rotor with Splitter Blades*, U.S. Army Research Laboratory, Mechanical Sciences Division, Research Triangle Park, Monterey, California, 2013.
21. A. Mehdi, *Effect of Swirl Distortion on Gas Turbine Operability*, Cranfield: School Of Engineering Power and Propulsion Department, Cranfield University, 2014.
22. A. Naseri, M. Boroomand, and S. Sammak, Numerical investigation of effect of inlet swirl and total-pressure distortion on performance and stability of an axial transonic compressor, *J. Thermal Science*, 2016, vol. 25, no. 6, pp. 501–510.
23. V. Iyengar, L.N. Sankar, and R. Denney, A first-principles based methodology for design of axial compressor configurations, in: *ASME: Power for Land, Sea, and Air*, vol. 6, Montreal, Canada, May 14–17, 2007.
24. S.L. Dixon, in: *Fluid Mechanics and Thermodynamics of Turbomachinery*, Burlington: Elsevier, 2005, pp. 16–22.
25. J. F. Hu, X. CH. Zhu, H. OuYang, X. Q. Qiang, and Zh.H. Du, Performance prediction of transonic axial compressor based on streamline curvature method, *J. Mechanical Science and Technology*, 2011, vol. 12, pp. 3037–3045.
26. C. Hah, A numerical modelling of endwall and tip clearance flow of an isolated compressor rotor, *J. Engineering and Gas Turbine*, 1986.